

# A high-resolution spectroscopic study of two new Na- and Al-rich field giants - likely globular cluster escapees in the Galactic halo

Avrajit Bandyopadhyay,<sup>1\*</sup> Sivarani Thirupathi,<sup>1</sup> Timothy C Beers<sup>2</sup> and A.Susmitha<sup>3</sup>

<sup>1</sup>*Indian Institute of Astrophysics, Bangalore, 560034 India*

<sup>2</sup>*Department of Physics and JINA Center for the Evolution of the Elements, University of Notre Dame, Notre Dame, IN, 46656, USA*

<sup>3</sup>*Tata Institute of Fundamental Research, Mumbai, 400005, India*

Accepted XXX. Received YYY; in original form ZZZ

## ABSTRACT

The stars SDSS J0646+4116 and SDSS J1937+5024 are relatively bright stars that were initially observed as part of the SDSS/MARVELS pre-survey. They were selected, on the basis of their weak CH *G*-bands, along with a total of 60 others, in the range of halo globular cluster metallicities for high-resolution spectroscopic follow-up as a part of the HESP-GOMPA survey (Hanle Echelle SPectrograph – Galactic survey Of Metal Poor stArs). The stars exhibit typical nucleosynthesis signatures expected from the so-called second-generation stars of globular clusters. The light-element anti-correlation of Mg-Al is detected, along with elevated abundances of Na. Carbon is found to be depleted, which is compatible with expectation. Lithium is also detected in SDSS J0646+4116 and SDSS J1937+5024; the measured abundances are similar to those of normal halo giant stars. These bright escapees provide a unique opportunity to study the nucleosynthesis events of globular clusters in great detail, and shed light on their chemical-enrichment histories.

**Key words:** stars: abundances stars: chemically peculiar stars: Population II Galaxy: halo (Galaxy:) globular clusters: general

## 1 INTRODUCTION

Globular clusters (GCs) are expected to lose a large amount of stellar mass during their interactions with the tidal field of the Milky Way (e.g., Baumgardt & Makino 2003; Kruijsen 2014; Martell 2018, and references therein). There are several processes by which stars can escape from GCs. The primary reason is their lower bounding energy, as they are of low mass due to the equipartition of energy, which in turn causes mass segregation. The various effects of mass segregation on the mass of escaping stars are investigated in Balbinot & Gieles (2018). Among many others, Baumgardt & Makino (2003) also discusses such effects on clusters embedded in tidal fields. Other processes, such as disc shocking and dynamical friction, can also contribute to the loss of stars from GCs. However, mass loss in Milky Way GCs due to dynamical friction would be negligible, as the mass loss in this scenario primarily depends on the Galactocentric distance of the cluster. Although disc/bulge shocks do produce enhanced mass loss (e.g., Dehnen et al. 2004), most of the mass loss is due to secular evolution. The importance

of each mass-loss process depends upon the properties of the cluster, as shown in the “vital diagram” of Gnedin & Ostriker (1997).

Chemical tagging is one of the important tools for identifying stars of GC origin among the halo field stars (Freeman & Bland-Hawthorn 2002). Although both the cluster and field populations exhibit similar elemental abundances of  $\alpha$ -, Fe-peak, and neutron-capture elements (Gratton et al. 2004; Pritzl et al. 2005; Lind et al. 2015), many stars in GCs exhibit certain unique trends for their light elements (C, N, O, Na, Mg, Al), uncharacteristic of the vast majority of halo stars (e.g., Kraft 1979; Kraft et al. 1979; Norris & Freeman 1979, and numerous references since). These traits are thought to emerge as a result of self pollution within the cluster, where the gas from the first generation of stars does not escape from the cluster, but instead pollutes the second-generation stars with the products of advanced hydrogen burning (Kraft et al. 1997; Carretta et al. 2009b,a). In hotter regions ( $T > 40$  MK), the Ne-Na chain begins converting  $^{20}\text{Ne}$  to  $^{23}\text{Na}$ , while simultaneously O is depleted via the ON cycle (Gratton et al. 2012). At still higher temperatures ( $T > 70$  MK), the Mg-Al cycle is initiated, which steadily depletes  $^{24}\text{Mg}$  and then  $^{25}\text{Mg}$  to  $^{27}\text{Al}$

\* E-mail: avrajit.india@gmail.com

(Denissenkov & Weiss 1996; Salaris & Weiss 2002). The sites where the C-N-O, Ne-Na, and Mg-Al cycles occur is the hot-bottom burning (HBB) regions (Bloeker & Schoenberner 1991; Boothroyd & Sackmann 1992) of the outer convective envelope of intermediate-to-high mass (3-8  $M_{\odot}$ ) AGB (IH-AGB) stars. Sufficiently high temperatures are not attained in the H-burning shells of low-mass RGB stars to sustain these reactions, hence no such variations are expected to be observed in halo field stars (Gratton et al. 2000).

Fast-rotating massive stars (FRMS) are also a probable site for similar nucleosynthesis reactions to take place (Decressin & Charbonnel 2007). The winds from these early generations of IH-AGB stars and FRMS alter the chemical composition of the birth clouds of subsequent generations of stars. Consequently, a large fraction of present-day GC stars are enhanced in Na and Al, along with depleted levels of C, O, and Mg. Almost all the Galactic GCs have been found to host multiple generations of stars (Bragaglia et al. 2017), as traced by the C-N-O anomaly (Kayser et al. 2008; Smolinski et al. 2011) and the anti-correlations of Na and O, and Mg and Al (e.g., Carretta et al. 2009a,b; Lee 2010; Martell & Grebel 2010; Martell 2011; Bragaglia et al. 2015; Carretta et al. 2017). The scenarios leading to the onset of the multiple stellar populations are highly debated; there could be several scenarios, as comprehensively discussed in Bastian & Lardo (2018).

Martell & Grebel (2010) demonstrated that  $\sim 2.5\%$  of  $\sim 2000$  low-metallicity halo giants studied by the SEGUE (Sloan Extension for Galactic Understanding and Exploration; Yanny et al. 2009) survey exhibited enhanced N and depleted C relative to the remaining field stars. A similar result was obtained by Martell et al. (2011) from SEGUE-II. Ramírez et al. (2012) discovered two field dwarfs showing the Na-O anti-correlations, which could be attributed to GC origin. Lind et al. (2015) found one star from the GAIA-ESO survey with Mg and Al abundances largely different from the halo population, but consistent with GC abundances. Halo giants with GC-like abundances of N and Al were also identified by Martell et al. (2016), using the SDSS APOGEE (Apache Point Galactic Evolution Experiment; Majewski et al. 2016) survey.

These studies have estimated that a substantial portion of the halo could have been contributed by GCs (e.g., Carretta et al. 2010; Ramírez et al. 2012; Lind et al. 2015), but consensus has not yet been reached regarding the precise fraction. Martell & Grebel (2010) and Martell (2011) estimated that 3% of the halo could have been contributed by GCs, consistent with the studies conducted by Carretta et al. (2010) and Ramírez et al. (2012). Martell et al. (2016) found 2% of their sample of halo stars to have the chemical signatures of second-generation GC stars, which corresponds to a much larger amount of total mass loss. Following Martell et al. (2011), the original contribution from GCs amounts to 13% of halo stars, in order to account for the 2% being chemically taggable as second-generation stars. From the DR14 release of SDSS-IV, Koch et al. (2019) have further refined the observed fraction of such objects to be 2.6%, bringing the original contribution from GCs to  $\sim 11\%$ .

Here we discuss the discovery of two likely second-generation GC escapees with enhanced Na, Al, and depleted C, O, and Mg.

## 2 OBSERVATIONS AND ANALYSIS

High-resolution ( $R \sim 30,000$ ) spectroscopic observations of our two program stars, SDSS J064655.6+411620.5 and SDSS J193712.01+502455.5 (hereafter J0646+4116 and J1937+5024) were carried out as a part of the GOMPA (Galactic survey Of bright Metal Poor stars) survey, using the Hanle Echelle Spectrograph on the 2-m Himalayan Chandra Telescope (HCT) at the Indian Astronomical Observatory (IAO). The targets for the HESP-GOMPA survey were selected from the spectroscopic pre-survey of MARVELS, which was carried out as a part of SDSS-III. This offers the opportunity to identify bright halo stars which could be studied at high spectral resolution using moderate-aperture telescopes. The pre-survey uses simple magnitude and color cuts ( $8 < V < 13$ ;  $B - V > 0.6$ ) to select targets suitable for the MARVELS RV survey. The survey fields are mostly low-latitude fields, which is suitable for exo-planet searches, but not ideal for detecting metal-poor stars. We have used synthetic spectral fitting of the pre-survey data to identify new metal-poor candidates (in the domain of GC metallicity;  $[\text{Fe}/\text{H}] > -2.5$ ) with weak CH  $G$ -bands, a well-known feature of GC stars that can be studied from low-resolution data (e.g., SDSS). We have obtained high-resolution data for 60 metal-poor stars in the metallicity range of GCs (the survey paper is in prep.). Two stars among them were found to be likely GC escapees – showing all the expected chemical signatures in their high-resolution spectra. The stars were observed at a spectral resolution of  $R \sim 30,000$  over the wavelength range 380nm to 1000 nm. Details of the observations, along with the signal-to-noise ratios and  $V$  magnitudes, for these two stars are listed in Table 1.

Data reduction was carried out using the IRAF echelle package, as well as the publicly available data reduction pipeline for HESP developed by Arun Surya. A cross-correlation analysis with a synthetic template spectrum was carried out to obtain the radial velocity (RV) for each star, listed in Table 1.

Photometric as well as Spectroscopic data have been used to estimate the stellar atmospheric parameters for these stars.  $T_{\text{eff}}$ ,  $\log(g)$ ,  $[\text{Fe}/\text{H}]$ , and microturbulent velocity. The abundances of individual elements present in each spectrum were determined using standard procedures, as described in Bandyopadhyay et al. (2018). Photometric temperatures were obtained using the available data in the literature and the standard  $T_{\text{eff}}$ -color relations derived by Alonso et al. (1996) and Alonso et al. (1999).  $T_{\text{eff}}$  estimates have also been derived spectroscopically, demanding that there be no trend of Fe I line abundances with excitation potential, as well as by fitting the  $H_{\alpha}$  profiles. The wings of  $H_{\alpha}$  are also sensitive to temperature. Estimates of surface gravity,  $\log(g)$ , for these stars were determined by the usual technique that demands equality of the iron abundances derived for the neutral (Fe I) lines and singly ionized (Fe II) lines. Parallaxes from Gaia have also been employed to derive the  $\log(g)$  for individual stars. The wings of the Mg I lines, which are sensitive to variations of  $\log(g)$ , have also been fitted to obtain the best-fit value. The plots for ionization balance and using Fe I and Fe II lines are shown in the top panels of Figure 1; fits for the Mg triplet and  $H_{\alpha}$  are shown in the middle panels for the two program stars. The wings

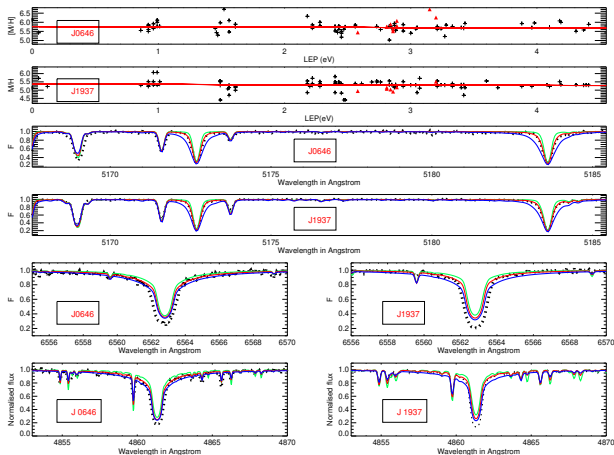


**Figure 1.** The stellar parameters for the two program giants. The upper panels display the ionization equilibrium plot, in which the best fit with the minimum slope and standard deviation among all the computed model stellar atmospheres for each star has been shown. Black crosses denote the Fe I abundances, while red filled triangles indicate the Fe II abundances. The middle panels show the fits in the spectral region of the Mg triplet for different values of  $\log(g)$  in steps of 0.75 dex; the best-fit value is marked in red for each star. The lower panels show the fits in the H- $\alpha$  region for different values of temperature in steps of 300K; the best-fit value is marked in red for each star. The bottom panels show the fits for the wings of H $\beta$ ; the best fit is marked in red, and is adopted as the stellar parameter of the star. The green and blue lines show the departure variation of temperature by 200K.

of the H $\beta$  line is sensitive to both variation in temperature and  $\log(g)$ . Spectral fits of H $\beta$  line are shown in the bottom panel of Figure 1, with the best fit marked in red. For determination of the stellar parameters, 81 and 99 Fe I lines and 12 and 8 Fe II lines could be measured for J0646+4116 and J1937+5024, respectively. The adopted values of the stellar parameters for both stars are shown in Table 1.

We have employed one-dimensional LTE stellar atmospheric models (ATLAS9; Castelli & Kurucz 2004) and the spectral synthesis code TURBOSPECTRUM (Alvarez & Plez 1998) for determining the abundances of the individual elements present in each spectrum. We have considered the equivalent widths of the absorption lines present in the spectra that are less than 120 mÅ, as they are on the linear part of the curve of growth. Version 12 of the turbospectrum code for spectrum synthesis and abundance estimates has been used for the analysis. We have adopted the hyperfine splitting provided by McWilliam (1998) and Solar isotopic ratios.

We have used the method of equivalent-width analysis for the clean, strong, and unblended lines of the light elements (such as C, N, and O), the  $\alpha$ -elements, and the Fe-peak elements. Spectral synthesis was carried out for the weaker features of these elements, and all lines of the neutron-capture elements, taking into account the hyperfine transitions where they are present. Solar abundances for the individual elements are taken from Asplund et al. (2009).

### 3 ABUNDANCES

#### 3.1 Light and $\alpha$ -Elements

Lithium was detectable for both J0646+4116 and J1937+5024. The strong Li doublet at  $\lambda 6707$  Å was used, from which we obtain abundances of  $A(\text{Li}) = 0.95$  and 1.05, respectively, similar to other evolved giants observed in the field.

Carbon abundances were measured by performing a spectral synthesis for the CH  $G$ -band region around  $\lambda 4313$  Å. The band head could be detected and measured in J0646+4116 and J1937+5024, yielding best-fit values of  $[\text{C}/\text{Fe}] = -0.02$  and  $[\text{C}/\text{Fe}] = -0.53$ , respectively. Corrections to the C abundances associated with the evolutionary state for each star (Placco et al. 2014) have also been computed<sup>1</sup>, and found to be +0.01 dex and +0.50 dex for J0646+4116 and J1937+5024, respectively.

Nitrogen abundances were obtained by measuring the CN molecular band at  $\lambda 3883$  Å. The C abundances obtained from the  $G$ -band were used, with a wide range of N abundances, and the best fit of the spectral band head was taken as the value of the N abundance. However, being close to the extreme blue end of the spectrum, the signal-to-noise in this region is poor, and thus only an upper limit could be derived for one of our stars, J1937+5024; it is found to be slightly enhanced, with a value of  $[\text{N}/\text{Fe}] < +0.42$ . Oxygen abundances were measured from the weak lines at  $\lambda 6300$  Å and  $\lambda 6363$  Å, which are regions that are heavily populated by atmospheric lines, thus telluric correction is vital for obtaining the correct values of oxygen. O abundances could be measured for J1937+5024 while an upper limit could be obtained for J0646+4116; both are found to be enhanced, with abundances of  $[\text{O}/\text{Fe}] = +0.31$  and  $[\text{O}/\text{Fe}] < +0.51$ , respectively.

Among the  $\alpha$ -elements, Mg and Ca could be measured for both the stars, while the Si lines were too weak to derive any meaningful abundances for either. Several lines for Mg and Ca could be obtained throughout the spectra, of which only the clean lines were used to derive the abundances. The very strong lines, such as the Mg triplet around  $\lambda 5172$  Å, were ignored in the computation of the abundances. J0646+4116 is found to have  $[\text{Ca}/\text{Fe}] = +0.23$  and  $[\text{Mg}/\text{Fe}] = +0.21$ , while J1937+5024 has  $[\text{Ca}/\text{Fe}] = +0.21$  and  $[\text{Mg}/\text{Fe}] = +0.30$ , which are somewhat lower than the typical  $\alpha$ -element enhancement of +0.4 dex in halo stars. Calcium could be taken as the true representative of the  $\alpha$ -elements, as other species, such as O, Si, and Mg are often altered due to the recycling of the products of an earlier generation of stars during subsequent star formation inside GCs (Kraft et al. 1997; Gratton et al. 2004; Carretta et al. 2010; Gratton et al. 2012).

Na and Al are the most important among the odd- $Z$  elements to tag a star of GC origin, and both were detected for our stars. Aluminium abundances have been derived by spectral fitting of the strong resonance line at  $\lambda 3961$  Å, while the D1 and D2 lines at  $\lambda 5890$  Å and  $\lambda 5896$  Å were used for deriving abundances of Na. Na line at  $\lambda 8194.8$  Å could also be detected. The spectral fits for Al are shown in Figure 2. The NLTE corrections for this line could be rather high,

<sup>1</sup> <http://vplacco.pythonanywhere.com/>

close to +1.0 dex, as discussed by [Baumüller & Gehren \(1997\)](#), [Andrievsky et al. \(2008\)](#), and [Nordlander & Lind \(2017\)](#). The NLTE corrections for Na ([Andrievsky et al. 2007](#)) have also been taken into account, and incorporated in the final values.

### 3.2 Fe-Peak Elements

The abundances of Cr, Co, Mn, Ni, and Zn could be measured by the usual equivalent-width analysis of the clean lines. Non-LTE corrections for each species (where available) have been incorporated in the final abundances. Cr and Co also suffer from large NLTE corrections, which could be a reason for the over-abundance (e.g., [Bergemann & Cescutti 2010](#)).

The two odd-Z elements Mn and Cu show the usual deficiency with respect to Fe in the metal-poor domain, as found in previous studies of halo and GC stars. However, Ni is found to be rather high for J1937+5024. Three lines of Ni could be detected at  $\lambda 4401.538 \text{ \AA}$ ,  $\lambda 4459.027 \text{ \AA}$ , and  $\lambda 5476.920 \text{ \AA}$ ; the Ni line at  $\lambda 4459.027 \text{ \AA}$  yielded an anomalously high abundance. Considering the other two lines, the abundance of Ni is based on the other two lines, yielding  $[\text{Ni}/\text{Fe}] = +0.21$  and  $[\text{Ni}/\text{Fe}] = +0.28$  for J0646+4116 and J1937+5024, respectively. The discrepancy in the Ni abundance due to the spectral line at  $\lambda 4459.027 \text{ \AA}$  requires further investigation.

The identical trends for Fe-peak elements in GCs and halo field stars indicate that they likely had a similar pre-enrichment history during the epoch of formation in the early phases of Galactic chemical evolution.

### 3.3 Neutron-Capture Elements

The neutron-capture elements Sr and Ba could be measured for both the program stars, and found to have normal abundances without notable irregularities. The resonance lines of Sr II at  $\lambda 4077 \text{ \AA}$  and  $\lambda 4215 \text{ \AA}$  were used to derive the Sr abundances, while the resonance lines at  $\lambda 4554 \text{ \AA}$  and  $\lambda 4934 \text{ \AA}$  were measured to determine the Ba abundances. Spectral synthesis was employed to derive both abundances, taking into account the hyperfine transitions. Spectral fits for Ba are shown in Figure 2 for both program stars.

The complete abundance tables for J0646+4116 and J1937+5024 are provided in Tables 2 and 3 respectively.

## 4 RESULTS AND DISCUSSION

Both of our program stars exhibit enhancement in  $[\text{Na}/\text{Fe}]$  and  $[\text{Al}/\text{Fe}]$  compared to halo stars of similar metallicity. They also show an under-abundance of  $[\text{C}/\text{Fe}]$ , along with depletion in  $[\text{O}/\text{Fe}]$ , which is compatible with second-generation GC stars.  $[\text{Mg}/\text{Fe}]$  is also found to be depleted in J0646+4116 and J1937+5024. Since elements such as C, O, and Mg could be significantly altered during quiescent burning in proton-fusion reactions ([Gratton et al. 2004](#)), Ca should be adopted as the best representative of the  $\alpha$ -elements for comparison with halo-star abundances. The degree of  $\alpha$ -element enhancement based on the Ca abundances is found to be slightly lower than is typical for halo stars, at  $[\alpha/\text{Fe}] = +0.22$ .

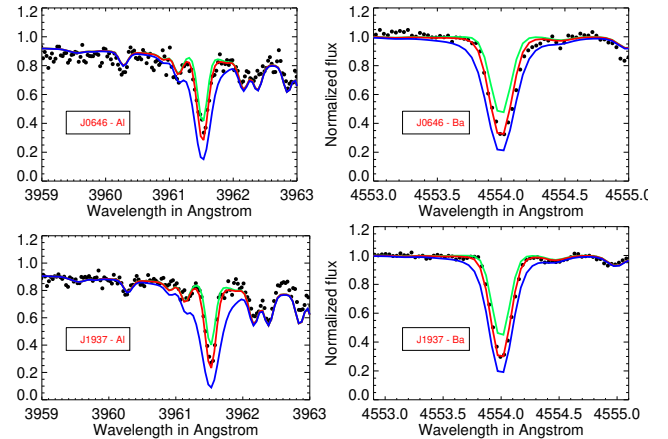


**Figure 2.** The left panels show the fits for Al, while the right panels show the fits for Ba. The red lines denote the best-fit abundances, over-plotted with two synthetic spectra of abundances 0.25 dex higher and lower in blue and green, respectively. The names of the program stars and corresponding synthesized elements are provided in each panel.

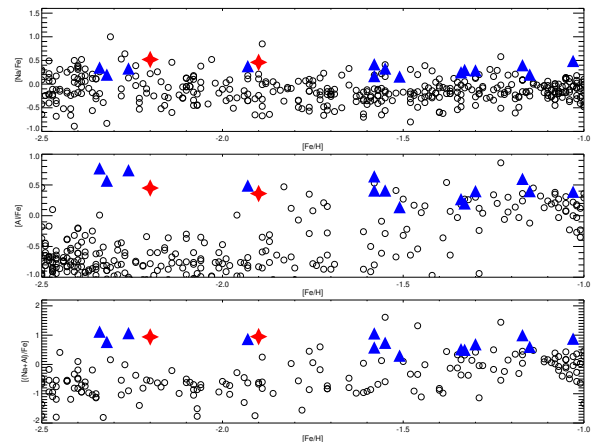


**Figure 3.** A comparative study on the light-element abundances for GCs and halo stars. The blue upward triangles indicate mean GC abundances, whereas the open circles indicate the halo stars. The two program stars discussed here are marked with red filled stars. The three panels show the distribution of the key elements Na and Al with metallicity. Our program stars consistently fall in the domain of GC abundances in all the plots. The data for GCs are taken from Carretta et al. (2009a), and the abundances for halo stars are taken from the SAGA database (Suda et al. 2008).

We have conducted a comparative study of the light-element abundances for our program stars with stars from the halo population and GC abundances, as shown in Figure 3. The abundances for the GC population are based on the UVES spectra of 19 Galactic GCs, as reported by [Carretta et al. \(2009a\)](#) while the abundances for halo stars are taken from the SAGA database ([Suda et al. 2008](#)). The top and middle panels display the enhancement in  $[\text{Na}/\text{Fe}]$  and  $[\text{Al}/\text{Fe}]$ , with respect to  $[\text{Fe}/\text{H}]$ , for GC stars and halo stars. To more clearly separate the GC population from the halo stars, we have also plotted  $[(\text{Na}+\text{Al})/\text{Fe}]$  vs.  $[\text{Fe}/\text{H}]$  in the



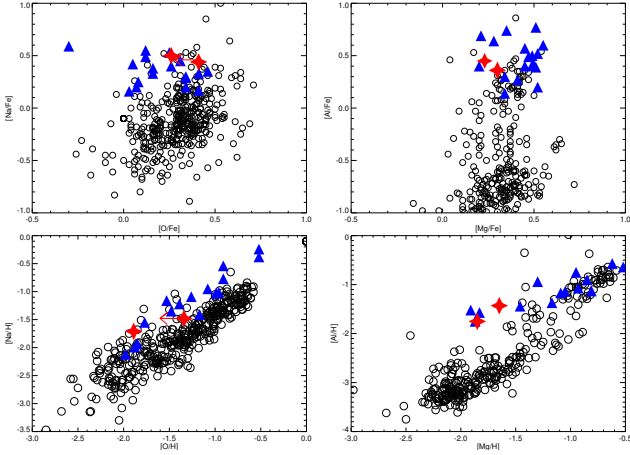


**Figure 4.** The top two panels show the Na-O and Mg-Al anti-correlations. The two panels at the bottom probe the origin of light-element anti-correlations by removing the dependence on metallicity. The red arrow indicates the obtained upper limit for O abundances in the case of J0646+4116. The data for GCs are taken from Carretta et al. (2009b), and the abundances for halo stars are taken from the SAGA database (Suda et al. 2008). The symbols are the same as in Figure 3.

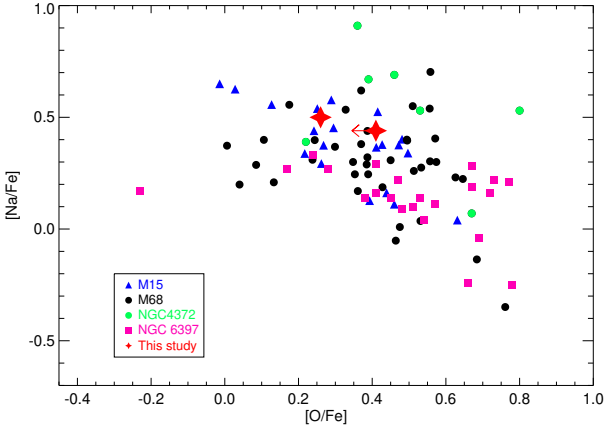


**Figure 5.** Comparison of the abundances of the two halo field giants with the other metal poor globular cluster in the same range of metallicity namely M15, M68, NGC 4372 AND NGC 6397 along the Na-O anticorrelation. The abundances of the individual stars in these GCs have been compiled as follows - M15 were obtained from Carretta et al. (2009b) ; M68 were taken from Lee et al. (2004) and Carretta et al. (2009a); NGC 4372 were obtained from San Roman, I. et al. (2015); NGC 6397 were taken from Carretta et al. (2009b), Lind, K. et al. (2011) and Pasquini, L. et al. (2008).

bottom panel. Both the program stars fall in the domain of GC abundances in these plots.

We note that the observed enhancement in  $[\text{Na}/\text{Fe}]$  and  $[\text{Al}/\text{Fe}]$  could also arise if these stars were members of the thick disc, but such stars are expected to show a much higher metallicity than our program stars, and are also inconsistent with the C and O abundances. The space velocities have also been determined for the target stars, and are found to be consistent with space velocities for halo stars (Kinman et al.

2007). The values of  $u, v$  and  $w$  for J1937+5024 are -165.4, -172.9, and -92.3 while for J0646+4116 they are found to be 330.3 -275.3 and -57.0. Figure 4 in Kinman et al. (2007) shows the distribution of stars, based on their space velocities, and classifies them into prograde and retrograde orbits. J1937+5024 is consistent with the halo stars with prograde orbits, while J0646+4116 falls very close to the edge of the line separating prograde motion from retrograde motion. Both of the program stars are on halo-like orbits. Thus, thick-disc membership appears improbable from the consideration of both abundances and space velocities.

To strengthen the argument, we have also tried to look for the Na-O and Mg-Al anti-correlations in Figure 4. The data for GCs are taken from Carretta et al. (2009a), and the abundances for halo stars are taken from the SAGA database (Suda et al. 2008). Though we could only obtain an upper limit for O in J0646+4116 the abundances fit better with the GC population. In the bottom panels of Figure 4, we attempt to probe the existence of these anti-correlations by removing the trends with metallicity. In the  $[\text{Al}/\text{H}]$  vs.  $[\text{Mg}/\text{H}]$  plane, the GCs and the likely escapees still stand out from the halo population, and exhibit a different trend in the distribution, whereas an offset could be seen with a similar trend between the GCs and halo population in the  $[\text{Na}/\text{H}]$  vs.  $[\text{O}/\text{H}]$  plane.

Figure 5 provides a comparison of the abundances of our two program stars with individual GC stars of similar metallicity from M15, M68, NGC 4372 and NGC 6397; the Na-O anticorrelation is clear. The abundances of the individual stars in these GCs have been compiled as follows - M15 were obtained from Carretta et al. (2009a) ; M68 were taken from Lee et al. (2004) and Carretta et al. (2009a); NGC 4372 were obtained from San Roman, I. et al. (2015); NGC 6397 were taken from Carretta et al. (2009a), Lind, K. et al. (2011) and Pasquini, L. et al. (2008). The position of the target stars in the Na-O plane is found to be well within the scatter of the GC stars of similar metallicity.

Lithium could also be detected in both the program stars, and is found to be normal. Li is a fragile element, which is completely destroyed in a temperature range much lower than that required for operation of Mg-Al cycle. Thus, the presence of Li in second-generation stars indicates heavy dilution of the gas processed by p-capture reactions with unprocessed gas that still preserves the standard Population II lithium abundance (D’Antona et al. 2019).

In the case of AGB stars, Li could also be produced by Cameron & Fowler (1971) mechanism in the envelope of the star at the early stages of the HBB phase (mass loss during the Li-rich phase of the AGB is discussed in detail in Ventura, P. & D’Antona, F. (2005)). D’Antona et al. (2019) shows the classic dilution scheme for the abundance of Li in second-generation GC stars using AGB ejecta and mixing with primordial gas. As observed by D’Orazi et al. (2014) and D’Orazi et al. (2015), the first generation (FG) and the second generation (SG) stars in M12 and NGC 362 exhibit the same Li abundance, which indicates the presence of a progenitor population like AGB stars that can produce Li. However, the simple dilution model fails to explain the internal variation and complex Li abundances in some of the GCs, like NGC 1904 and NGC 2808 – the production

efficiency of Li also depends upon the cluster’s mass and metallicity (D’Orazi et al. 2015). Li have been measured in several Galactic globular clusters; the Li abundances exhibit a similar distribution as normal halo stars.

## 5 CONCLUSION

A sample of  $\sim 60$  stars in the domain of GC metallicity with weak carbon molecular CH  $G$ -bands selected from the low-resolution SDSS/MARVEL pre-survey have been observed at high spectral resolution to identify signatures of second-generation stars in GCs. Two such stars were found to be consistent with all of the expected light-element anomalies. The stars studied here are most likely to be GC escapees. Binary mass transfer from an intermediate AGB or direct pollution from a massive star wind might be unlikely to have caused the abundance anomaly due to the presence of lithium in both these objects. Upcoming massive spectroscopic surveys will identify more such objects. GAIA kinematics and accurate ages from asteroseismology will throw light on the origin and frequency of such objects.

## 6 ACKNOWLEDGEMENT

We thank the referee for useful comments that helped clarify the presentation and enhance the quality of the paper. We are particularly thankful to the referee for suggesting the addition of Figure 5. We thank the staff of IAO, Hanle and CREST, Hosakote, that made these observations possible. The facilities at IAO and CREST are operated by the Indian Institute of Astrophysics, Bangalore. We also thank Prof. Piercarlo Bonifacio for his valuable comments and suggestions. T.C.B. acknowledges partial support from grant PHY 14-30152 (Physics Frontier Center/JINA-CEE), awarded by the U.S. National Science Foundation (NSF). T.C.B. also acknowledges partial support from the Leverhulme Trust (UK), which hosted his visiting professorship at the University of Hull during the completion of this study.

**Table 1.** Observational Details for our Program Stars

Object	RA	DEC	Exposure (secs)	Frames	SNR	V (mag)	Radial Vel. (km s <sup>-1</sup> )	$T_{\text{eff}}$ (K)	log(g) (cgs)	$\xi$	[Fe/H]
SDSS J064655.6+411620.5	06 46 55.6	+41 16 20.5	2400	6	43	11.14	-285.0	5150	2.25	1.50	-1.90
SDSS J193712.0+502455.5	19 37 12.01	+50 24 55.50	2400	3	130	10.44	-184.0	4800	1.50	1.50	-2.20

**Table 2.** Elemental Abundances for SDSS J064655.6+411620.5

Name	Species	Solar	lines	A(X)	[X/H]	[X/Fe]	$\sigma^*$
Li	Li I	...	1	0.95	...	...	0.03
C	CH	8.43	...	6.25	-2.18	-0.02	0.05
O	O I	8.69	1	7.30	-1.39	+0.51	0.09
Na	Na I	6.24	2	4.75	-1.49	+0.41	0.08
Mg	Mg I	7.60	5	5.91	-1.69	+0.21	0.06
Al	Al I	6.45	1	4.92	-1.53	+0.37	0.11
Ca	Ca I	6.34	10	4.67	-1.67	+0.23	0.08
Sc	Sc II	3.15	3	1.72	-1.43	+0.47	0.04
Ti	Ti I	4.95	8	3.47	-1.47	+0.43	0.05
	Ti II	4.95	14	3.57	-1.38	+0.52	0.07
Cr	Cr I	5.64	5	3.80	-1.84	+0.06	0.09
	Cr II	5.64	3	4.06	-1.58	+0.32	0.07
Mn	Mn I	5.43	3	3.24	-2.19	-0.29	0.12
Co	Co I	4.89	2	2.62	-2.27	-0.37	0.08
Ni	Ni I	6.22	3	4.56	-1.66	+0.24	0.07
Zn	Zn I	4.56	2	2.89	-1.67	+0.23	0.06
Sr	Sr II	2.87	2	1.25	-1.62	+0.28	0.05
Ba	Ba II	2.18	3	0.75	-1.43	+0.47	0.03

**Table 3.** Elemental Abundances for SDSS J193712.01+502455.5

Name	Species	Solar	lines	A(X)	[X/H]	[X/Fe]	$\sigma^*$
Li	Li I	...	1	1.05	...	...	0.02
C	CH	8.43	...	6.00	-2.43	-0.53	0.03
N	CN	7.83	...	6.05	-1.78	+0.42	0.15
O	O I	8.69	1	6.80	-1.89	+0.31	0.07
Na	Na I	6.24	2	4.50	-1.74	+0.46	0.03
Mg	Mg I	7.60	5	5.80	-1.80	+0.30	0.02
Al	Al I	6.45	1	4.70	-1.75	+0.45	0.07
Ca	Ca I	6.34	7	4.35	-1.99	+0.21	0.07
Sc	Sc II	3.15	3	0.95	-2.20	+0.00	0.02
Ti	Ti I	4.95	7	3.14	-1.81	+0.39	0.04
	Ti II	4.95	14	2.86	-2.09	+0.11	0.04
Cr	Cr I	5.64	5	3.33	-2.31	-0.11	0.04
	Cr II	5.64	4	3.35	-2.29	-0.09	0.06
Mn	Mn I	5.43	3	2.77	-2.66	-0.46	0.12
Co	Co I	4.89	2	2.68	-2.31	-0.11	0.03
Ni	Ni I	6.22	2	4.70	-1.52	+0.28	0.04
Zn	Zn I	4.56	2	2.37	-2.19	+0.01	0.02
Sr	Sr II	2.87	2	0.75	-2.12	+0.08	0.02
Ba	Ba II	2.18	3	0.25	-1.93	+0.27	0.02

## REFERENCES

- Alonso A., Arribas S., Martínez-Roger C., 1996, *A&A*, **313**, 873
- Alonso A., Arribas S., Martínez-Roger C., 1999, *A&AS*, **140**, 261
- Alvarez R., Plez B., 1998, *A&A*, **330**, 1109
- Andrievsky S. M., Spite M., Korotin S. A., Spite F., Bonifacio P., Cayrel R., Hill V., François P., 2007, *A&A*, **464**, 1081
- Andrievsky S. M., Spite M., Korotin S. A., Spite F., Bonifacio P., Cayrel R., Hill V., François P., 2008, *A&A*, **481**, 481
- Asplund M., Grevesse N., Sauval A. J., Scott P., 2009, *ARA&A*, **47**, 481
- Balbinot E., Gieles M., 2018, *MNRAS*, **474**, 2479
- Bandyopadhyay A., Sivarani T., Susmitha A., Beers T. C., Giridhar S., Surya A., Masseron T., 2018, *ApJ*, **859**, 114
- Bastian N., Lardo C., 2018, *Annual Review of Astronomy and Astrophysics*, **56**, 83
- Baumgardt H., Makino J., 2003, *MNRAS*, **340**, 227
- Baumüller D., Gehren T., 1997, *A&A*, **325**, 1088
- Bergemann M., Cescutti G., 2010, *A&A*, **522**, A9
- Bloecker T., Schoenberner D., 1991, *A&A*, **244**, L43
- Boothroyd A. I., Sackmann I.-J., 1992, *ApJ*, **393**, L21
- Bragaglia A., Carretta E., Sollima A., Donati P., D’Orazi V., Gratton R. G., Lucatello S., Sneden C., 2015, *A&A*, **583**, A69
- Bragaglia A., Carretta E., D’Orazi V., Sollima A., Donati P., Gratton R. G., Lucatello S., 2017, *A&A*, **607**, A44
- Cameron A. G. W., Fowler W. A., 1971, *ApJ*, **164**, 111
- Carretta E., et al., 2009a, *A&A*, **505**, 117
- Carretta E., Bragaglia A., Gratton R., Lucatello S., 2009b, *A&A*, **505**, 139
- Carretta E., Bragaglia A., Gratton R. G., Recio-Blanco A., Lucatello S., D’Orazi V., Cassisi S., 2010, *A&A*, **516**, A55
- Carretta E., Bragaglia A., Lucatello S., D’Orazi V., Gratton R. G., Donati P., Sollima A., Sneden C., 2017, *A&A*, **600**, A118
- Castelli F., Kurucz R. L., 2004, *ArXiv Astrophysics e-prints*,
- D’Antona F., Ventura P., Marino A. F., Milone A. P., Tailo M., Criscienzo M. D., Vesperini E., 2019, *The Astrophysical Journal*, **871**, L19
- D’Orazi V., Angelou G. C., Gratton R. G., Lattanzio J. C., Bragaglia A., Carretta E., Lucatello S., Momany Y., 2014, *The Astrophysical Journal*, **791**, 39
- D’Orazi V., et al., 2015, *Monthly Notices of the Royal Astronomical Society*, **449**, 4038
- Decressin T., Charbonnel C., 2007, in Kerschbaum F., Charbonnel C., Wing R. F., eds, *Astronomical Society of the Pacific Conference Series Vol. 378, Why Galaxies Care About AGB Stars: Their Importance as Actors and Probes*. p. 54
- Dehnen W., Odenkirchen M., Grebel E. K., Rix H.-W., 2004, *The Astronomical Journal*, **127**, 27532770
- Denissenkov P. A., Weiss A., 1996, *A&A*, **308**, 773
- Freeman K., Bland-Hawthorn J., 2002, *ARA&A*, **40**, 487
- Gnedin O. Y., Ostriker J. P., 1997, *ApJ*, **474**, 223
- Gratton R. G., Sneden C., Carretta E., Bragaglia A., 2000, *A&A*, **354**, 169
- Gratton R., Sneden C., Carretta E., 2004, *ARA&A*, **42**, 385
- Gratton R. G., Carretta E., Bragaglia A., 2012, *A&A Rev.*, **20**, 50
- Kayser A., Hilker M., Grebel E. K., Willemsen P. G., 2008, *A&A*, **486**, 437
- Kinman T. D., Cacciari C., Bragaglia A., Buzzoni A., Spagna A., 2007, *MNRAS*, **375**, 1381
- Koch A., Grebel E. K., Martell S. L., 2019, *A&A*, **625**, A75
- Kraft R. P., 1979, *ARA&A*, **17**, 309
- Kraft R. P., Trefzger C. F., Suntzeff N., 1979, in Burton W. B., ed., *IAU Symposium Vol. 84, The Large-Scale Characteristics of the Galaxy*. pp 463–473
- Kraft R. P., Sneden C., Smith G. H., Shetrone M. D., Langer G. E., Pilachowski C. A., 1997, *AJ*, **113**, 279
- Kruijssen J. M. D., 2014, *Classical and Quantum Gravity*, **31**, 244006
- Lee J.-W., 2010, *MNRAS*, **405**, L36
- Lee J.-W., Carney B. W., Habgood M. J., 2004.
- Lind, K. Charbonnel, C. Decressin, T. Primas, F. Grundahl, F. Asplund, M. 2011, *A&A*, **527**, A148
- Lind K., et al., 2015, *A&A*, **575**, L12
- Majewski S. R., APOGEE Team APOGEE-2 Team 2016, *Astronomische Nachrichten*, **337**, 863
- Martell S. L., 2011, *Astronomische Nachrichten*, **332**, 467
- Martell S. L., 2018, in Chiappini C., Minchev I., Starkenburg E., Valentini M., eds, *IAU Symposium Vol. 334, Rediscovering Our Galaxy*. pp 38–42 ([arXiv:1710.03858](https://arxiv.org/abs/1710.03858)), doi:10.1017/S1743921317007487
- Martell S. L., Grebel E. K., 2010, *A&A*, **519**, A14
- Martell S. L., Smolinski J. P., Beers T. C., Grebel E. K., 2011, *A&A*, **534**, A136
- Martell S. L., et al., 2016, *ApJ*, **825**, 146
- McWilliam A., 1998, *AJ*, **115**, 1640
- Nordlander T., Lind K., 2017, *A&A*, **607**, A75
- Norris J., Freeman K. C., 1979, *ApJ*, **230**, L179
- Pasquini, L. Ecuivillon, A. Bonifacio, P. Wolff, B. 2008, *A&A*, **489**, 315
- Placco V. M., Frebel A., Beers T. C., Stancliffe R. J., 2014, *ApJ*, **797**, 21
- Pritzl B. J., Venn K. A., Irwin M., 2005, *AJ*, **130**, 2140
- Ramírez I., Meléndez J., Chanamé J., 2012, *ApJ*, **757**, 164
- Salaris M., Weiss A., 2002, *A&A*, **388**, 492
- San Roman, I. et al., 2015, *A&A*, **579**, A6
- Smolinski J. P., Martell S. L., Beers T. C., Lee Y. S., 2011, *AJ*, **142**, 126
- Suda T., et al., 2008, *PASJ*, **60**, 1159
- Ventura, P. D’Antona, F. 2005, *A&A*, **431**, 279
- Yanny B., et al., 2009, *AJ*, **137**, 4377